Production and Properties of Biaxially Oriented Polyethylene Tubes

A. K. TARAIYA and I. M. WARD*

IRC in Polymer Science & Technology, University of Leeds, Leeds LS2 9JT, United Kingdom

SYNOPSIS

A study of the production of biaxially oriented polyethylene tubes by the die-drawing process was carried out examining the effects of draw temperature, haul-off speed, and mandrel size. The effect of postmandrel cooling was also studied. A range of biaxially oriented tubes of various draw ratios and thicknesses were produced. The Young's modulus and the tensile strength of biaxially drawn samples show considerable enhancement in both directions over the isotropic material. Biaxially drawn samples show remarkable improvement in their impact strength over the isotropic material. The crystalline orientation and texture of these samples are characterized using wide-angle X-ray scattering pole figure analysis.

INTRODUCTION

The die-drawing process was developed in this laboratory to produce thick uniaxially or biaxially oriented products.[1-6] Earlier efforts to produce oriented polymer tubes in this laboratory were concerned with the hydrostatic extrusion process. Hope et al.[7] demonstrated that by using a stationary mandrel and converging die arrangement, round tubular products can be satisfactorily hydrostatically extruded, although the extrusion speeds achieved at the higher extrusion ratios were disappointingly low, generally in the order of only a few millimeters per minute. These very low production speeds together with the batch nature of the process have limited the development of the hydrostatic extrusion process for industrial purposes. To exploit the enhancement of mechanical and physical properties associated with oriented polymer tubes produced at an industrially acceptable rate, the die-drawing technique was adopted for tube drawing. Die drawing is a technique that combines the best features of free tensile drawing and solid-state extrusion, allowing a large-section product to be made at high modulus levels obtainable by free drawing. In the case of uniaxial drawing of a rod, a heated polymer billet is drawn through a heated conical die by applying a pulling force on the billet at the exit side of the die. The polymer billet is free to neck down and follows an optimum strain and strain rate path through the die, leaving the die wall at an appropriate point and hence considerably reducing the required flow stress. The same principle was applied for the uniaxial drawing of the tubes with reduced bore. This process was modified for expanded bore tube drawing by using the conical expanded mandrel. In several previous articles the preparation of oriented tubes of polyethylene terephthalate,[4] polyvinylchloride,[5] polypropylene,[6] and polyphenylenesulfide[8] by die drawing was described. The present article describes the production of biaxially oriented polyethylene tubes with their mechanical and structural properties.

EXPERIMENTAL

Batch Die-Drawing Rig

Early patented work in this department on biaxial drawing of tubes describes processes in which the tubular material is drawn through a die and over an expanding mandrel.[9] In the case of expanded tube drawing, the hoop draw ratio of the product varies from the inner to the outer wall. These draw ratios are defined as:

* To whom correspondence should be addressed.

Journal of Applied Polymer Science, Vol. 59, 627–638 (1996)
 CCC 0021-8995/96/040627-12

$$\lambda_{hoop,inner} = \frac{\text{product ID}}{\text{billet ID}}$$

$$\lambda_{hoop,outer} = \frac{\text{product OD}}{\text{billet OD}}.$$

The axial draw ratio of the drawn tube is defined as the ratio of the cross-sectional area of the tubular billet to that of the drawn tube, that is,

$$\lambda_{axial} = \frac{(\text{billet OD})^2 - (\text{billet ID})^2}{(\text{product OD})^2 - (\text{product ID})^2}.$$

The batch die-drawing rig has been described in some detail elsewhere.[10] Early biaxially drawn tubes produced on the batch-drawing rig were often curved along their length and were nonround along their cross section. It was suspected that this was due to a top to bottom temperature gradient in the oven, and possibly also due to a gravitational effect. By rotating the grips, mandrel, mandrel rod, and tubular billet during the heating up and drawing, these drawbacks should be eliminated in the batch process. The existing batch die-drawing facility for drawing tubes has been modified accordingly and is shown in Figure 1. The drawing force is measured by a travelling load cell attached to a chain haul-off. Between the load cell and the drawn tube a coupling is fitted that has a thrust bearing to take the axial drawing load and allows the drawn tube to rotate. A pin is fitted to this assembly to enable it to be quickly attached to the tube. A steel rod attached to the conical mandrel passes back through the undrawn tubular billet and is anchored to the draw bench at the rear of the heaters. The anchor point is fitted with a thrust bearing and timing belt pulley so that the whole assembly can be rotated during both the warm up and the drawing period. Reduction gearing enables the motor to rotate the mandrel assembly at slow speed (25 rpm).

Materials

Commercially available polyethylene Rigidex 002-40 tubes with inner diameter (ID) of 25 mm and outside diameter (OD) of 32 mm were used. Polyethylene Rigidex 002-40 is a copolymer ($\sim$ 4 butyl branches/1000 carbon atoms), M_w = 182,600 and M_n = 20,500.

Drawing over an Expanded Mandrel

The tooling configuration for the expanded bore tube drawing is shown in Figure 1. A centering ring with 32-mm bore was used as a die and the tubular billet was drawn freely over the mandrel. The mandrel was kept inside the heating chamber up to the leading end. The gap between the exit end of the mandrel and the heating chamber was sealed.

The starting procedure for producing biaxially oriented tubes has been described in some detail in previous publications. In the case of polyethylene, the one end of the tubular billet was deformed at 115°–120°C to fit over the conical mandrel to start the drawing. The drawing was performed at various temperatures ranging from 90° to 120°C. Mandrel sizes from 45 to 70 mm were used to give different hoop draw ratios. The mandrel and billet chamber were heated to the desired drawing temperature. Billets were allowed about 2 h to attain thermal

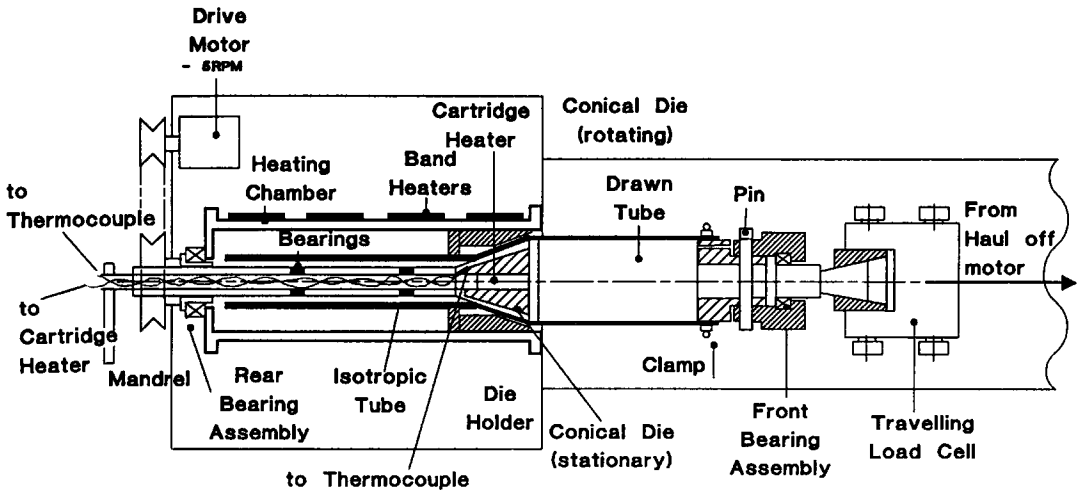

Figure 1 Plan of modified draw bench with rotating mandrel assembly.

equilibrium before starting the drawing. The mandrel and billet were rotated during the heating up and the drawing. The drawing was always started at a very slow speed, 1 cm/min. After stabilizing the drawing load, the drawing speed was then increased to the desired value. The drawing load was monitored throughout the run.

X-Ray Diffraction Measurements

The wide-angle X-ray $\theta/2\theta$ scans were taken in the angular ranges 15–30° in reflection geometry with a Huber texture goniometer employing CuKα radiation.

The wide-angle X-ray scattering (WAXS) patterns of biaxially drawn tubes were obtained using a flat-film camera with CuKα radiation generated at 40 kV and 30 mA. Photographs were recorded with the incident X-ray beam normal to the tube surface and parallel to the axial and hoop directions.

To describe the orientations of the crystallographic axes of crystallites in a polymeric material, a three-dimensional coordinate system is introduced, as shown in Figure 2. Sample reference coordinate axes have been defined along the machine direction (M), transverse direction (T), and normal direction (N). For biaxially drawn tubular samples the machine direction is the axial direction and the transverse direction is the hoop direction. The orientation of a unit vector normal to a given crystallographic plane can then be described by two angles α and β, where α is the angle between ON and the normal to the reflecting plane, and β is the angle between the projection of that normal on the OMT plane and the OT direction (see Fig. 2).

$I(\alpha, \beta)$ is the intensity representing the relative amount of material having (hkl) plane normals in direction α, β. Then

$$\langle \cos^2\theta_{hkl,N} \rangle = \frac{\int_0^{2\pi}\int_0^{\pi/2} I(\alpha,\beta)\cos^2\alpha \sin\alpha \, d\alpha \, d\beta}{\int_0^{2\pi}\int_0^{\pi/2} I(\alpha,\beta)\sin\alpha \, d\alpha \, d\beta}$$

$$\langle \cos^2\theta_{hkl,T} \rangle = \frac{\int_0^{2\pi}\int_0^{\pi/2} I(\alpha,\beta)\sin^3\alpha \cos^2\beta \, d\alpha \, d\beta}{\int_0^{2\pi}\int_0^{\pi/2} I(\alpha,\beta)\sin\alpha \, d\alpha \, d\beta}$$

$$\langle \cos^2\theta_{hkl,M} \rangle = \frac{\int_0^{2\pi}\int_0^{\pi/2} I(\alpha,\beta)\sin^3\alpha \sin^2\beta \, d\alpha \, d\beta}{\int_0^{2\pi}\int_0^{\pi/2} I(\alpha,\beta)\sin\alpha \, d\alpha \, d\beta}.$$

In the absence of strong meridional reflections in biaxially oriented polyethylene samples, it is necessary to determine the crystalline orientation factor, $\langle \cos^2\theta_{c,i} \rangle$, indirectly from equatorial reflections. For this study the (110) and (200) reflections were used. The calculations were carried out using Wilchinsky's method.[11]

Pole figure analysis and the determination of orientation functions of certain semicrystalline polymers are well documented in the literature.[12,13] X-ray measurements were made with a computer controlled Huber texture goniometer employing CuKα radiation. Samples, 30 × 20 mm, were cut from the biaxially drawn thin tubes and stuck flat on the sample holder to perform the X-ray scans.

Each sample was scanned to measure the intensity as a function of α and β in both transmission and reflection modes, because neither mode can cover the whole range of α from 0 to 90°. The position of the detector was set at the 2θ angle corresponding to a selected ($hk0$) reflection, while the sample was tilted and rotated about its own axis to record the intensities of the diffracting planes in space. The intensities were recorded with circular scans, for example β scans, at 10° intervals over the angular range $0° \leq \alpha \leq 90°$ and 2° intervals over the angular range $0° \leq \beta \leq 360°$. Circular scans were performed by the reflection technique for α = 0–50° and in transmission for α = 50–90°.

The intensity data was corrected for background, defocusing, and absorption effects. Background scatter was measured as a function of α and β at a 2θ position off the peak in reflection and transmission geometry. Defocusing and absorption corrections in reflection geometry were carried out using

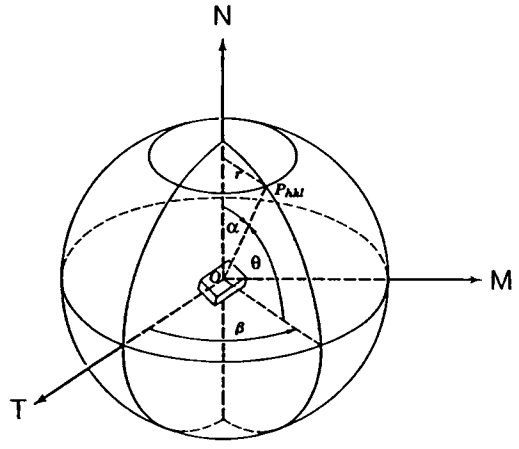

Figure 2 Position of pole P located by spherical coordinates α and β.

a random sample of the same thickness. Absorption corrections in transmission geometry were carried out according to a procedure developed by Decker et al.[14]

After applying the corrections, the intensities obtained from the transmission and reflection measurements were scaled to the same level.

Mechanical Properties

The tensile behavior of these samples was studied on an Instron tensile testing machine. Dumbbell shaped samples were cut from the tube in both the axial and hoop direction for testing. Tensile strength and percentage elongation at break were measured at 100% per minute strain rate. Measurements of the 10-s creep modulus at 0.1% strain were made with laboratory built equipment[15] on narrow strips of material cut from the drawn tubes in both the axial and hoop directions. The standard 10-s loading, 100-s recovery procedure was followed.

The impact behavior of these samples at 20°C was studied using the ROSAND instrumented impact tester. The tubes were slit open, flattened, and clamped in a circular grip. In this apparatus a 10-mm diameter hemispherical dart indentor is attached via a fast acting force transducer to a 10-kg weight that falls on the specimen from a height of 46 cm. The velocity at impact is therefore 3 m/s and the total energy available greatly exceeds that at which the specimen will fail. A measure of the force applied to the indentor by the specimen during the few milliseconds of impact is recorded and directly monitored as a force–time curve. The energy absorbed during the test is calculated from this force–time curve.

Some tests have been carried out on the short-term burst strength of isotropic and drawn tubes. The short-term pressure burst test conducted on these samples followed closely the ASTM standard D1599. All tests were carried out at 20° ± 1°C and the tubes were pressurized using water. Great care was taken to ensure that no air was trapped within the entire pressure test setup.

Oxygen Permeability

The permeability measurements were made by a continuous flow technique with the MOCON Oxtran 100 permeability equipment. In this method a continuous flow of gas is maintained on both sides of the barrier material. Initially, nitrogen gas is passed over both surfaces to remove oxygen in the sample. The nitrogen on one side is then replaced by oxygen, and the nitrogen flow on the other side then sweeps the surface to extract any oxygen that diffuses through the material. The diffusing oxygen is measured by a detector that is sensitive only to oxygen. Tubular samples were slit open flat and placed in the Oxtran cell.

RESULTS AND DISCUSSION

General Features of Die Drawing

The variations in the axial and the average hoop draw ratios with drawing speed at 100°, 110°, and 120°C for a 55-mm mandrel are shown in Figure 3. The axial draw ratio increases with drawing speed, and the hoop draw ratio decreases as the tube draws down after leaving the mandrel at all draw temperatures. The axial draw ratio is higher at lower draw temperatures at any given draw speed. The drawing load increases with a decrease in draw temperature. Some idea of the drawing behavior on the mandrel can be obtained by stopping the drawing and after cooling, sectioning, and measuring the material that remains on the mandrel. The procedure is not rigorously accurate because the material might relax due to a sudden change in load at stop, but casual observations of the neck at this time show that it does not alter significantly. The axial and hoop draw ratio variation over a 55-mm mandrel is shown in Figure 4. It can be seen from this figure that up to a certain distance prior to necking, the tube draws over the expanding mandrel only in the hoop direc-

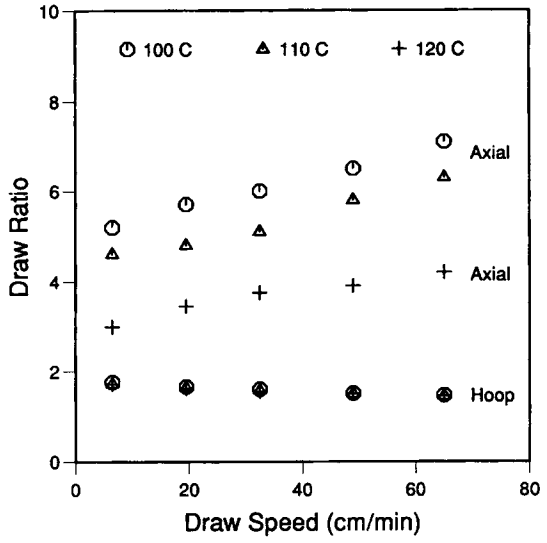

Figure 3 Variation in the axial and hoop draw ratios with drawing speed.

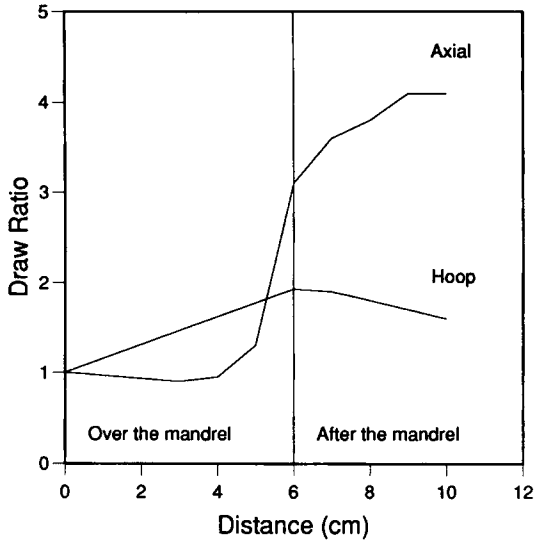

Figure 4 Variation of draw ratio over the 55-mm mandrel.

tion and contracts in the axial direction; hence, uniaxial drawing occurs in the hoop direction. At the neck, material begins to extend axially, while the hoop draw ratio is governed by the mandrel shape.

The hoop draw ratio decreases with drawing speed as the tube draws down after leaving the mandrel. This loss of hoop expansion can be minimized by cooling the product as it leaves the mandrel. For this purpose a 10-cm long vacuum operated water cooler was designed. This water cooler was placed next to the mandrel end and the product was drawn through it. The cooling water was at room temperature and circulated through the cooler at the rate of 2 L/min. The effect of cooling on the product diameter drawn at 120°C over the 55-mm mandrel is shown in Figure 5. It can be seen that by cooling the product as it leaves the mandrel most of the hoop expansion can be retained even at the high drawing speeds. The axial draw ratio also dropped on cooling from 4.4 to 2.3 at a draw speed of 65 cm/min. This suggests that the less unbalanced samples can be produced at higher draw speed by effectively cooling the product as it leaves the mandrel.

To get more hoop expansion the tubular billet was drawn over the 70-mm mandrel at 115°C. The mandrel was continuously heated and the temperature monitored throughout the drawing experiment. The variation of axial and hoop draw ratios with drawing speed are shown in Figure 6. A sample was drawn at 90°C over the 70-mm mandrel. All these samples drawn using the rotating system showed a marked improvement in both straightness of tube and uniformity of wall thickness when compared with the product drawn without rotation.

X-Ray Measurements

The 2θ scans for isotropic and samples drawn at 90°, 100°, and 120°C are shown in Figure 7. For an isotropic sample and a sample drawn at 120°C, the positions of the 2θ peaks correlate well with values for the polyethylene orthorhombic unit cell (a = 0.741, b = 0.492, and c = 0.254 nm). An additional peak that appears in a 2θ scan of the sample drawn

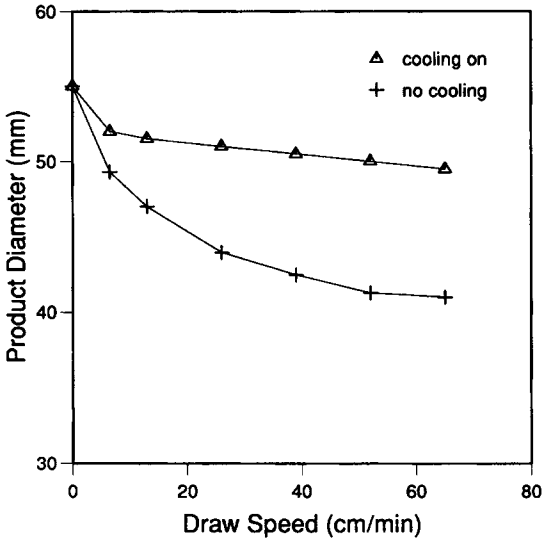

Figure 5 The effect of postmandrel cooling on the product diameter with drawing speed.

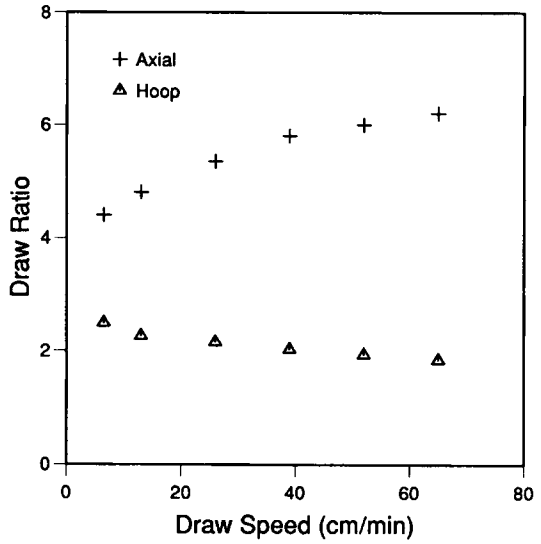

Figure 6 The variation of axial and hoop draw ratios with drawing speed. Mandrel size 70 mm, draw temperature 115°C.

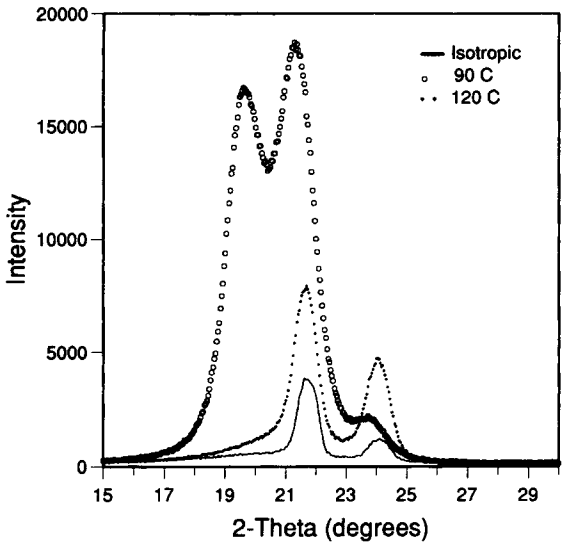

Figure 7 WAXS 2θ scans in reflection geometry of PE samples. Isotropic, drawn at 90° and 120°C.

at 100°C at $2\theta = 19.7$ is due to the (010) reflection of the monoclinic phase. The amount of the monoclinic phase increases as the sample is drawn at a lower temperature of 90°C. It is known that a certain amount of monoclinic phase ($a = 0.809$, $b = 0.479$, $c = 0.253$ nm, and $\gamma = 107.9°$) is produced when polyethylene is submitted to compression.[16]

There have been several detailed studies of the texture produced by solid-state deformation of polyethylene.[17-22] Two types of texture can be seen in drawn polyethylene sheets. In both of these the c axes are aligned parallel to the draw direction, but in the one the (100) planes are in the plane of the sheet (designated (100)[001] texture) and in the other the (110) planes are in the plane of the sheet (designated (110)[001] texture). The (100)[001] texture develops as a result of slip on the (100) planes. The presence of (110)[001] texture could possibly arise from three different mechanisms: (110) slip, (110), or (310) twinning. The pole positions from these mechanisms are given in Table I.

Figure 8 shows WAXS patterns of the biaxially drawn samples drawn at 120°C. WAXS patterns taken with the X-ray beam normal to the tube surface show that the (200) reflection is very faint, i.e. aligning preferably in the plane of the sample. The arc of the (110) reflection on the equator narrows as the axial draw ratio increases. WAXS patterns taken with the X-ray beam parallel to the hoop direction show that at a draw ratio 3.4 × 1.7 the equatorial reflections (110) and (200) split into three, at the equator and at about 25° on either side of it. As the axial draw ratio increases they merge back to give strong reflections at the equator. WAXS patterns taken with the X-ray beam parallel to the axial direction show that the (110) reflections have higher intensity at ~ 55° from either side of the equator. These WAXS patterns suggest the presence of (200) planar orientation. The WAXS pattern of a sample drawn at 90°C ($\lambda = 5.3 \times 2.2$) taken with the X-ray beam parallel to the axial direction show the presence of (110) planar orientation together with a significant presence of monoclinic phase as shown in Figure 9.

X-ray pole figures for the (200) and (110) reflections of samples drawn at 120°C are shown in Figures 10 and 11. These pole figures confirm the observations made from the WAXS patterns. Low draw ratio samples drawn at 120°C produced a tilted (100)[001] texture with the c axis tilted around 25° from the draw direction toward the normal direction; at high draw ratios the tilt decreased. X-ray pole figures for the (200) and (110) reflections of sample drawn at 90°C are shown in Figure 12. These pole figures show that only the (110)[001] texture is present. To confirm these findings, ω scans were carried out. The geometry for the ω scan is shown in Figure 13. ω is the angle between the film plane and the normal to the diffraction plane, $\omega = 90 - \alpha$. The ω scans over (200) and (110) reflections of samples drawn at 90° and 120°C are shown in Figures 14 and 15. In the ω scans of a sample drawn at 90°C, (200) shows maxima at 34° and (110) shows two maxima at 23 and 90°. This confirms that only (110)[001] texture is present in this sample. Of the ω scans of a sample drawn at 120°C, (200) shows a very broad peak at 90° and (110) shows two broad maxima at about 30° (due to merging of two peaks at 23 and 34°) and 90°. This confirms that both (100)[001] and (110)[001] textures are present in this sample.

Samples drawn at the lower temperature of 90°C require a high drawing stress (30 MPa). If the

Table I Pole Positions due to Different Textures in Polyethylene

Texture	Reflection	α (°)
(100)[001]	(200)	0
	(110)	56
(110)[001]	(200)	56
	(110)	0 and 67
(110) twinning on	(200)	0 and 67
(200)[001]	(110)	11 and 56
(310) twinning on	(200)	0 and 54
(200)[001]	(110)	2, 56, and 70

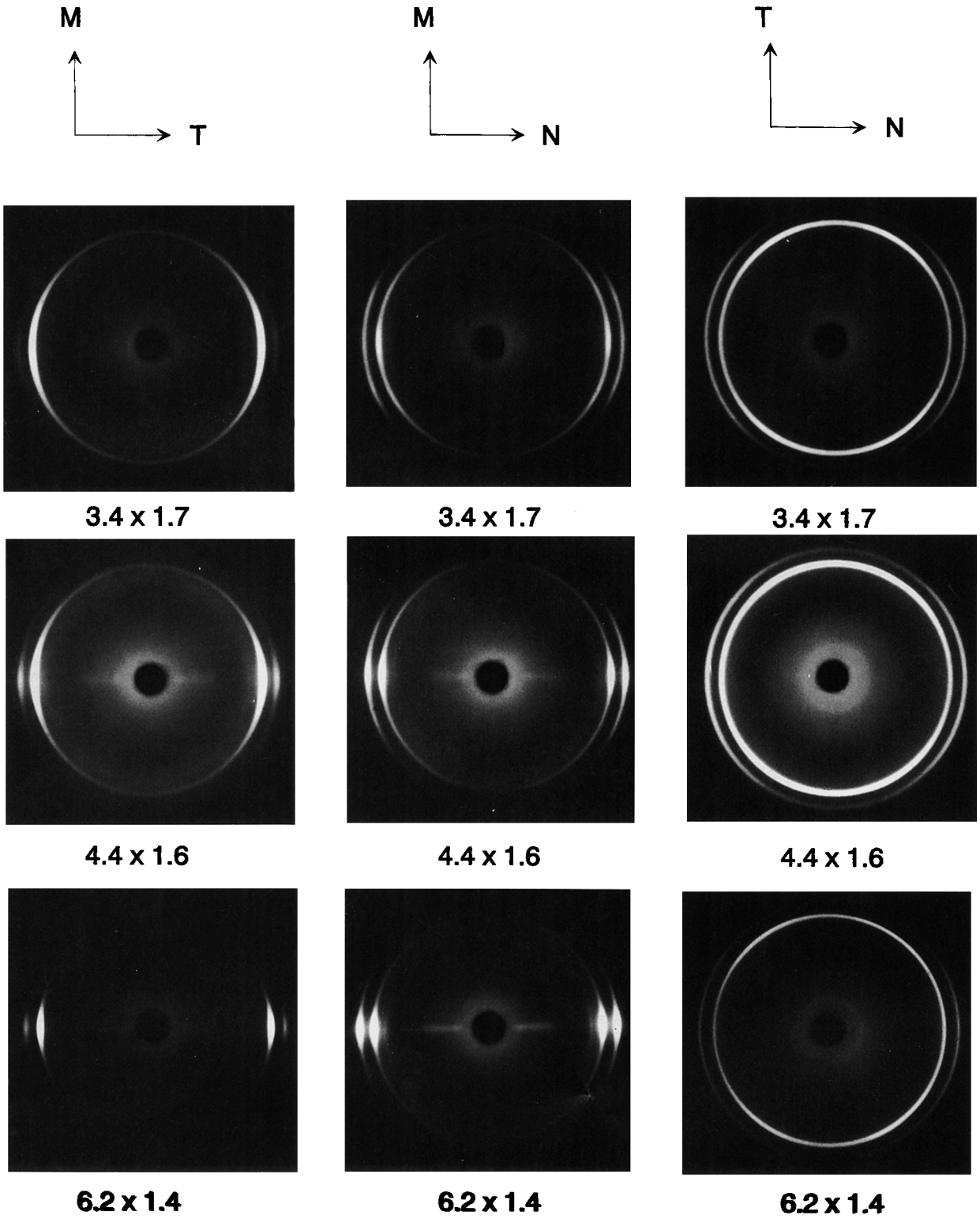

Figure 8 WAXS patterns of samples drawn at 120°C.

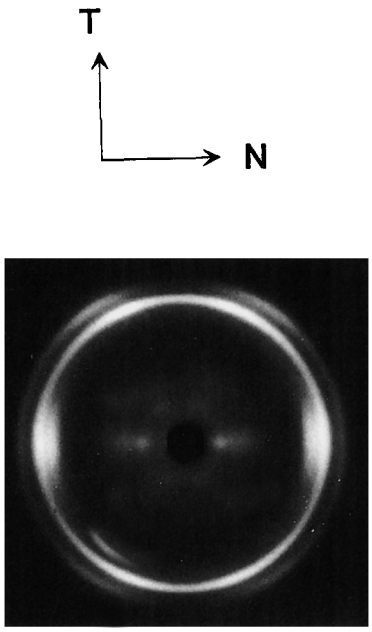

Figure 9 WAXS patterns of samples drawn at 90°C.

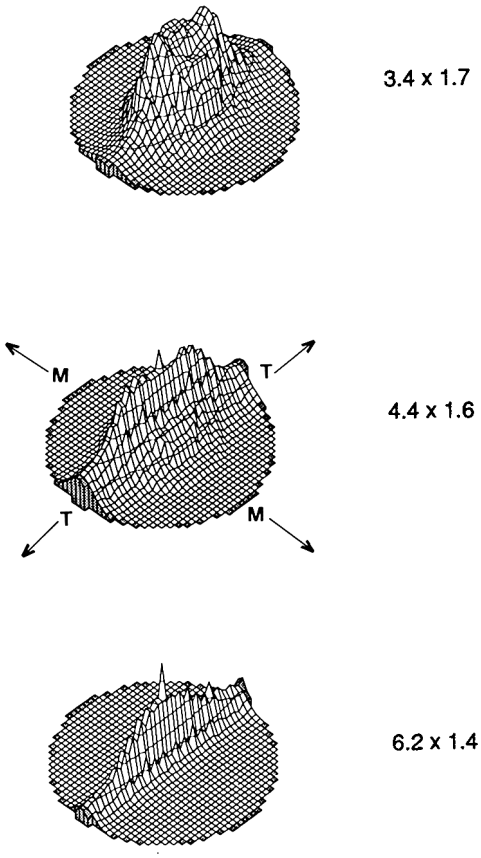

Figure 10 (200) pole figures of samples drawn at 120°C.

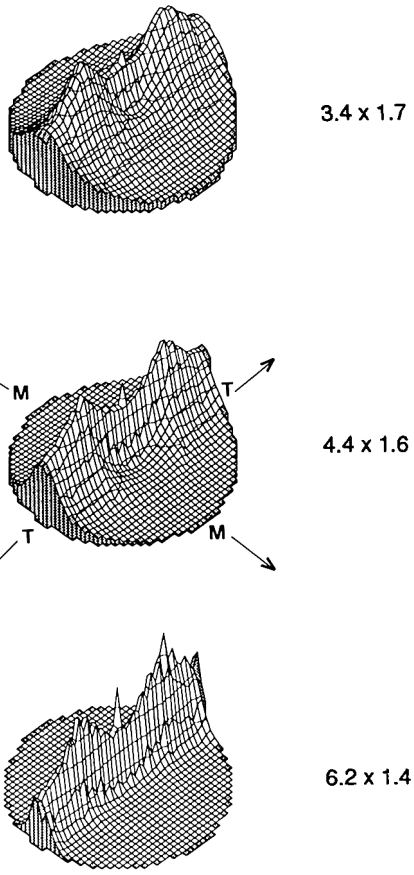

Figure 11 (110) pole figures of samples drawn at 120°C.

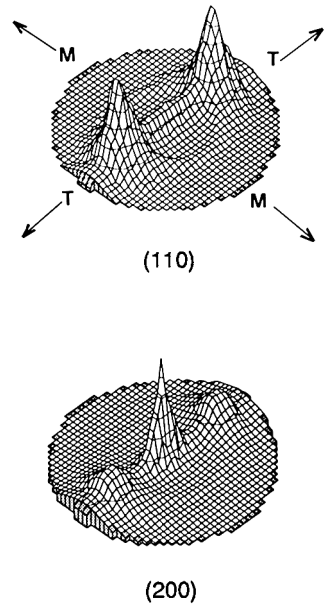

Figure 12 (110) and (200) pole figures of samples drawn at 90°C.

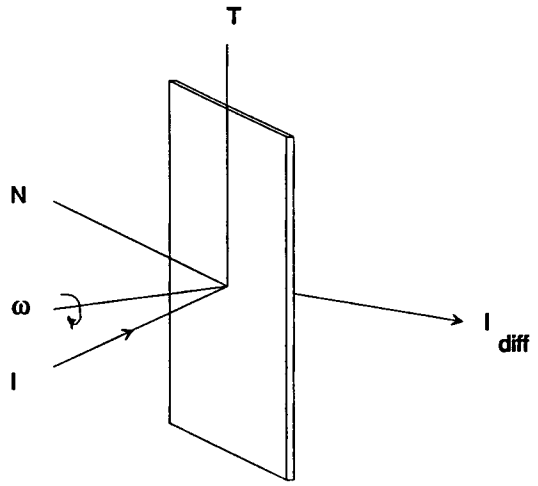

Figure 13 Geometry for ω scan.

drawing stress is high enough to activate (110)[001], slip then this should be the preferred mode of deformation because the (110) plane exhibits the greatest density of molecules in the plane and the greatest spacing between successive molecular planes. Samples drawn at 120°C require a low drawing stress (5 MPa), and in these samples (100)[001] slip is the preferred mode of deformation.

The results for *c* axis and *a* axis orientation averages for the samples drawn at 120°C are given in Tables II and III, respectively. All these biaxially drawn tubes are more drawn in the axial direction than in the hoop direction and this shows in their *c*-axis orientation averages. The *a* axis orientation

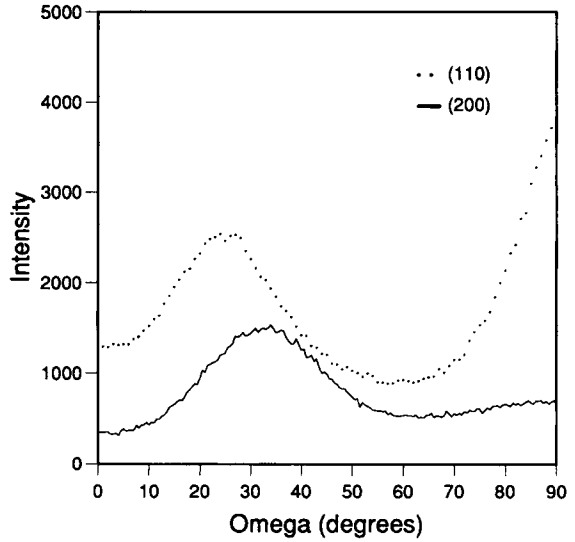

Figure 14 ω scans over (200) and (110) reflections for the sample drawn at 90°C.

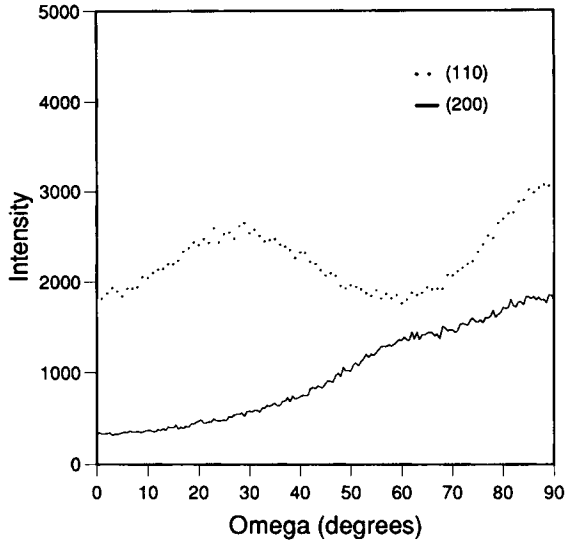

Figure 15 ω scans over (200) and (110) reflections for the sample drawn at 120°C.

averages in the normal direction are greater than in the machine and the transverse direction, i.e. the *a* axis is preferentially oriented normal to the plane of the film, meaning that the crystallographic (200) planes have a tendency to be oriented parallel to the film plane.

Mechanical Properties and Oxygen Permeability

The results for tensile properties are shown in Table IV. Axial tensile strength increases with axial draw

Table II Crystalline *c*-Axis Orientation Averages

Draw Ratio Axial × Hoop	$\langle\cos^2\theta_{c,M}\rangle$	$\langle\cos^2\theta_{c,T}\rangle$	$\langle\cos^2\theta_{c,N}\rangle$
3.4 × 1.7	0.72	0.26	0.02
4.4 × 1.6	0.81	0.15	0.04
5.2 × 1.5	0.86	0.12	0.02
6.2 × 1.4	0.90	0.10	0.00

Table III Crystalline *a*-Axis Orientation Averages

Draw Ratio Axial × Hoop	$\langle\cos^2\theta_{a,M}\rangle$	$\langle\cos^2\theta_{a,T}\rangle$	$\langle\cos^2\theta_{a,N}\rangle$
3.4 × 1.7	0.09	0.25	0.66
4.4 × 1.6	0.06	0.32	0.62
5.2 × 1.5	0.07	0.30	0.63
6.2 × 1.4	0.02	0.33	0.65

Table IV Tensile Properties and Burst Strength of Biaxially Drawn Polyethylene Tubes

Draw Ratio		Tensile Strength (MPa)		% Elongation at Break		Modulus (GPa)		Hoop Strength at Burst σ_h (MPa)
Axial	Hoop	Axial	Hoop	Axial	Hoop	Axial	Hoop	
1.0	1.0	22	22	700	700	0.5	0.5	20
2.9	1.6	86	34	260	550	0.7	0.7	32
4.1	1.6	98	40	100	550	1.2	0.9	—
4.9	1.6	114	44	80	500	1.4	1.0	—
3.4	1.7	95	37	150	500	0.7	0.7	35
4.4	1.6	110	42	95	480	0.95	0.8	38
5.2	1.5	120	40	80	500	1.15	0.95	—
6.2	1.4	140	39	75	520	1.35	1.1	—

ratio. The tensile strength in the hoop direction also increases slightly due to the increase in axial draw ratio where the average hoop draw ratio is the same. The tensile strength shows a reasonable correlation with draw ratio as can be seen in Figure 16. Percentage elongation at break decreases with an increase in draw ratio in both directions.

The result for the 10-s creep modulus are also given in Table IV and shown in Figure 17. It can be seen that the modulus in the axial direction increases with draw ratio. The modulus in the hoop direction is not independently related to hoop draw ratio, but is also influenced by the sample's axial draw ratio. In Figure 18 the modulus in the axial direction is plotted against the orientation average $\langle \cos^2\theta_{c,M} \rangle$. This shows a reasonable correlation between the modulus and the orientation of the c axes.

On impact at 20°C the isotropic and biaxially drawn samples showed ductile failures. The results for impact energy are shown in Table V. Biaxially drawn tubes show a remarkable improvement in their impact strength over the isotropic material.

An internal pressure test on the isotropic tube at room temperature shows characteristic beak-type failure at a hoop stress of 20 MPa. A thin biaxially drawn tube expands by a greater amount before bursting. Failures were parallel to the axial direction. Fractures were arrested after relatively short lengths and the splits had rounded ends. Photographs of these samples are shown in Figure 19. The hoop

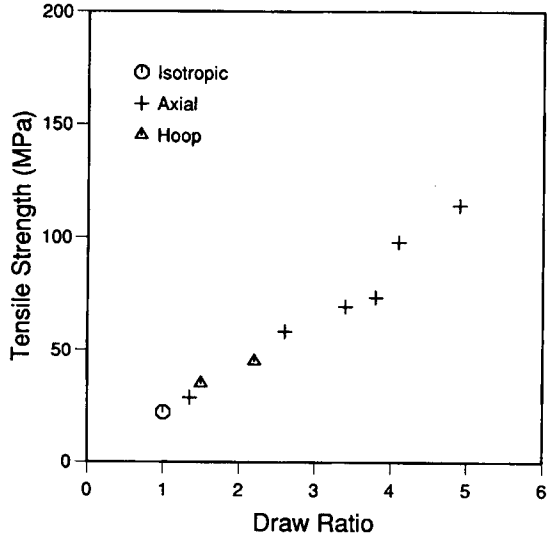

Figure 16 The effect of draw ratio on the tensile strength.

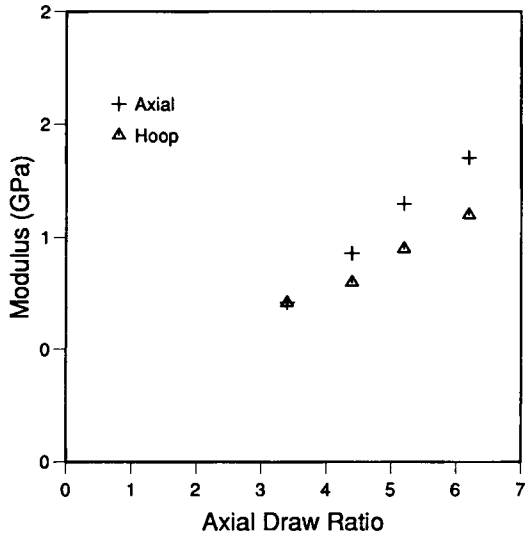

Figure 17 The effect of draw ratio on the modulus.

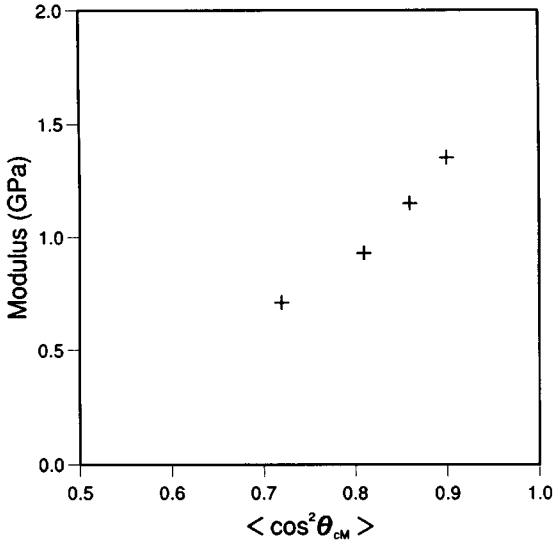

Figure 18 Variation of axial modulus with $\langle \cos^2\theta_{c,M} \rangle$.

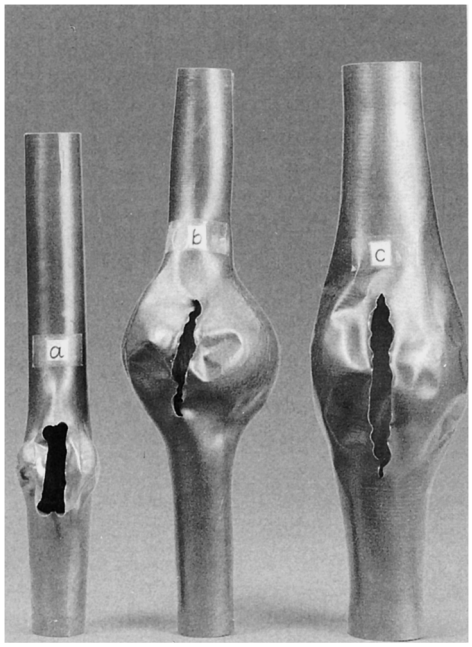

Figure 19 Samples after 60-s internal pressure burst test. Draw ratios (a) 1.8 × 1.5, (b) 3.4 × 1.7, (c) 4.4 × 2.2.

stress at failure of these samples were calculated as follows:

$$\sigma_h = \frac{PD}{2t}$$

where σ_h = hoop stress, P = internal pressure, D = average internal diameter, and t = wall thickness. Results for the hoop stress at burst were found to be similar to the tensile strength measured on an Instron for these samples as shown in Table IV.

Oxygen permeability results for isotropic and two biaxially drawn samples are given in Table VI. These results show that the biaxial drawing process reduces the permeability, but the reduction is not as great as in the case of uniaxial drawing. The major cause for such a small reduction in the permeability coefficient for oxygen in biaxially oriented polypropylene was found due to their low amorphous orientation.[23]

CONCLUSIONS

Uniform biaxially oriented tubes of various draw ratios and thicknesses are produced by the die-drawing process. A specimen drawn using the rotating system showed a marked improvement in both straightness of tube and uniformity of wall thickness when compared with the product drawn without rotation. Compared with isotropic material, biaxially oriented samples have a higher tensile strength and modulus in both directions. The impact strength of biaxially drawn samples is much better than that of the isotropic material. A sample drawn at 90°C (λ = 5.3 × 2.2) possesses only (110) planar orientation; for a sample drawn at 120°C (λ = 4.4 × 1.6), a mixed (100) and (110) planar orientation is present.

Table V Impact Energy of Biaxially Drawn Polyethylene Tubes

Draw Ratio Axial × Hoop	Thickness (mm)	E (J)
1.0 × 1.0	0.58	1.6
2.9 × 1.6	0.75	7.2
4.1 × 1.6	0.53	7.4
4.9 × 1.6	0.44	8.5
4.6 × 2.0	0.38	9.2

Table VI Oxygen Permeability Coefficient of Biaxially Drawn Polyethylene Tubes

Draw Ratio	P × 10^{11} cm^3 $cm/cm^2/(cm\ Hg)/s$
1.0 × 1.0	9.9
4.4 × 2.2	8.1
7.0 × 1.4	5.0

In this study we did not observed any significant influence of different textures on the mechanical properties of these samples. It appears that the mechanical properties are mainly affected by the orientation of the *c* axes.

REFERENCES

1. P. D. Coates and I. M. Ward, *Polymer,* **20,** 1553 (1979).
2. A. G. Gibson and I. M. Ward, *J. Mater. Sci.,* **15,** 979 (1980).
3. A. K. Taraiya, A. Richardson, and I. M. Ward, *J. Appl. Polym. Sci.,* **33,** 2559 (1987).
4. A. Selwood, I. M. Ward, and B. Parsons, *Plast. Rubber Proc. Appl.,* **8,** 49 (1987).
5. A. Selwood, A. K. Taraiya, I. M. Ward, and R. A. Chivers, *Plast. Rubber Proc. Appl.,* **10,** 85 (1988).
6. A. K. Taraiya and I. M. Ward, *Plast. Rubber Comp. Proc. Appl.,* **15,** 5 (1991).
7. P. S. Hope, A. G. Gibson, B. Parsons, and I. M. Ward, *Polym. Eng. Sci.,* **20,** 540 (1980).
8. P. L. Carr, D. W. Woods, and I. M. Ward, *Plast. Rubber Comp. Proc. Appl.,* **22,** 199 (1994).
9. A. Selwood and I. M. Ward, Br. Pat. 2,156,733 (1985).
10. A. Richardson, B. Parsons, and I. M. Ward, *Plast. Rubber Proc. Appl.,* **6,** 347 (1986).
11. Z. W. Wilchinsky, *Adv. X-ray Anal.,* **6,** 231 (1962).
12. L. E. Alexander, *X-ray Diffraction Methods in Polymer Science,* Wiley, New York, 1969.
13. D. Geiss and D. Hoffman, *Prog. Polym. Sci.,* **15,** 1 (1990).
14. B. F. Decker, E. T. Asp, and D. J. Harker, *Appl. Phys.,* **19,** 388 (1948).
15. V. B. Gupta and I. M. Ward, *J. Macromol. Sci. (Phys.),* **B1,** 373 (1967).
16. T. Seto, T. Hara, and K. Tanaka, *Jpn. J. Appl. Phys.,* **7,** 31 (1968).
17. F. C. Frank, A. Keller, and A. O'Connor, *Phil. Mag.,* **3,** 64 (1958).
18. M. Bevis and E. B. Crellin, *Polymer,* **12,** 666 (1971).
19. G. C. Adam, *J. Polym. Sci., Part A-2,* **9,** 1235 (1971).
20. M. H. Cho, S. Hibi, and T. Kyu, *J. Mater. Sci.,* **26,** 2507 (1991).
21. N. S. J. A. Gerrtis and R. J. Young, *J. Polym. Sci., Polym. Phys.,* **29,** 825 (1991).
22. L. Lin and A. S. Argon, *J. Mater. Sci.,* **29,** 294 (1994).
23. A. K. Taraiya, G. A. J. Orchard, and I. M. Ward, *J. Appl. Polym. Sci.,* **41,** 1659 (1990).

Received March 21, 1995
Accepted June 30, 1995